The RAMONES Service for Rapid Assessment of Seismic Moment and Radiated Energy in Central Italy: Concepts, Capabilities, and Future Perspectives

Daniele Spallarossa*[1,2], Matteo Picozzi[3], Davide Scafidi[1], Paola Morasca[2], Chiara Turino[1], and Dino Bindi[4]

Abstract
We present Rapid Assessment of MOmeNt and Energy Service (RAMONES), a service for disseminating through a web interface, the estimates of seismic moment (M0) and radiated energy (ER) for earthquakes occurring in central Italy with local magnitudes above 1.7. The service is based on a fully-automatic procedure developed for downloading and processing open seismological data from the European Integrated Data Archive, Italian Civil Protection repository, and Incorporated Research Institutions for Seismology (IRIS). In its actual configuration, RAMONES uses the seismic catalog generated through the event webservice of the Italian Institute of Geophysics and Volcanology (compliant with International Federation of Digital Seismograph Networks standards) to guide the data download. The concept of RAMONES is to estimate M_0 and E_R from features extracted directly from recordings, namely the S-wave peak displacement (PDS) and the integral of the squared velocity ($IV2_S$) evaluated over the S-wave window at local distances. A data set composed of 6515 earthquakes recorded in central Italy between 2008 and 2018 was used to calibrate the attenuation models relating M_0 to PD_S and E_R to $IV2_S$, including station corrections. The calibration values for M_0 and E_R were extracted from the source spectra obtained by applying a decomposition approach to the Fourier amplitude spectra known as the generalized inversion technique. To test the capabilities of RAMONES, we validate the attenuation models by performing residual analysis over about 60 earthquakes occurring in 2019 that were used for the spectral decomposition analysis but not considered in the calibration phase. Since January 2020, a testing operational phase has been running, and RAMONES has analyzed about 800 earthquakes by September 2020. The distribution of the source parameters and their relevant scaling relationships are automatically computed and disseminated in the form of maps, parametric tables, figures, and reports available through the RAMONES web interface.

Introduction

The long history of destructive earthquakes in Europe, where moderate events also can have tremendous effects due to the high density of populated areas and the high vulnerability of historical cities and settlements, led the seismological community to establish in 1975 the European–Mediterranean Seismological Centre (EMSC) to provide real-time parametric data for the European–Mediterranean region. More recently, the Observatories and Research Facilities for European Seismology (ORFEUS) was established (Nolet et al., 1986). The standardization of formats for data transmission and archiving (International Federation of Digital Seismograph Networks [FDSN], see Data and Resources) and the establishment of open repositories for sharing real-time and archived streams (see Data and Resources) had a strong impact on opening new scientific directions. If the development in data telemetry opened the new research field of real-time seismology (Kanamori, 2005), the availability of denser and high-quality seismic networks deployed near faults made possible the recording of very large numbers of micro and small earthquakes, pushing the seismological community to develop novel big data analysis strategies

(e.g., Ross et al., 2017, 2019; Zhu and Beroza, 2018; Kong et al., 2019; Mousavi, Zhu, Ellsworth, and Beroza, 2019; Mousavi, Zhu, Sheng, and Beroza, 2019; Münchmeyer et al., 2019; Scafidi et al., 2019). Within the current operational scenario by which large volumes of data from dense seismic networks can be fast accessed and processed, the development of services for rapid assessment of source parameters became feasible. Here, we present a service providing seismological products for characterizing the seismic source properties in central Italy, named Rapid Assessment of MOmeNt and Energy Service

1. DISTAV, University of Genoa, Genoa, Italy, https://orcid.org/0000-0002-8021-3908 (DSp); https://orcid.org/0000-0002-4872-0213 (DSc); 2. Istituto Nazionale di Geofisica e Vulcanologia (INGV), Milan, Italy, https://orcid.org/0000-0002-6525-4867 (PM); 3. University of Naples Federico II, Department of Physics, Naples, Italy; 4. Helmholtz Centre Potsdam, GFZ German Research Centre for Geosciences, Potsdam, Germany, https://orcid.org/0000-0002-8619-2220 (DB)

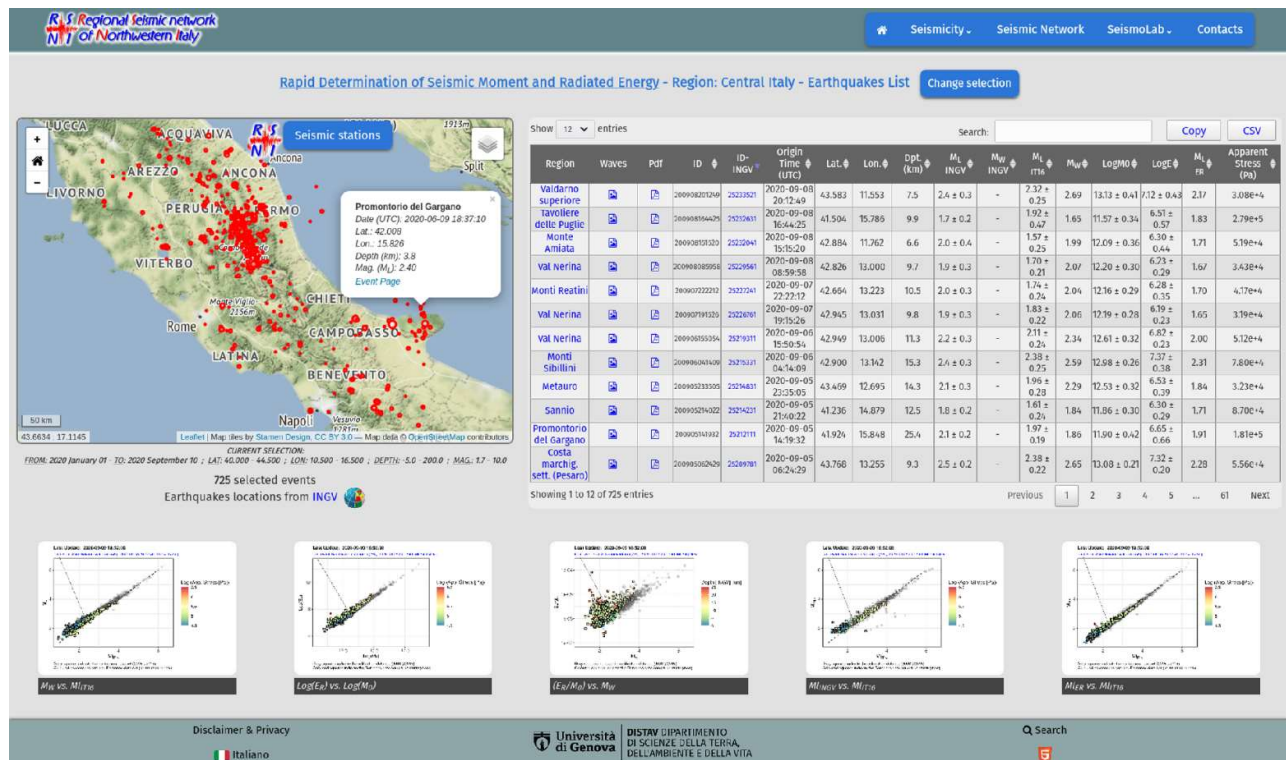**Corresponding author:* daniele.spallarossa@unige.it

Figure 1. Screenshot of the webpage relevant to the application of Rapid Assessment of MOmeNt and Energy Service (RAMONES) in central Italy (see Data and Resources). A map with locations and a table with source parameters are shown for earthquakes analyzed since January 2020. Within the table, a link to a specific event page (Fig. 2) is provided. Using the "Seismic stations" selections, a map of the station locations and relevant metadata is shown. Different scaling relationships are shown in figures refreshed following the RAMONES updates. See RAMONES Web Interface section for more details. INGV, National Institute for Geophysics and Volcanology.

(RAMONES). In its actual configuration, RAMONES uses information and data provided by services of the European Integrated Data Archive (ORFEUS-EIDA) and the Italian Civil Protection Department (DPC) to disseminate, among other parameters, estimates of the seismic radiated energy (E_R) and seismic moment (M_0) for earthquakes larger than $M_L \sim 1.7$ in central Italy. The parameters are computed using features extracted directly from recordings, and the outcomes are disseminated with an a priori fixed delay of one day with respect to the earthquake origin time. The need to develop a monitoring strategy for earthquake source parameters originated after the 2016–2017 central Italy seismic sequence that included three mainshocks (i.e., the M_w 6.2 Amatrice, M_w 6.1 Visso, and M_w 6.5 Norcia earthquakes that occurred between 24 August and 30 October 2016) and lead to recording more than 500,000 earthquakes through mid-2017 (e.g., Zhang et al., 2019; Spallarossa et al., 2020). RAMONES builds its strategy for the rapid and robust assessment of M_0 and E_R over previous studies performed in central Italy. For earthquake early warning purposes, Picozzi et al. (2017) proposed the estimation of the radiated seismic energy and seismic moment from P-wave signals for almost 40 earthquakes, including the largest magnitude events of the 2016–2017 central Italy seismic sequence. The authors showed that it was possible, by comparing the moment and the energy magnitude scales, to identify events with stress drops higher than the average, providing important information about the earthquake shaking potential. A further development was proposed by Bindi et al. (2018), who focused on S-wave windows of more than 1400 earthquakes in the magnitude range of $2.5 \leq M_w \leq 6.5$, recorded by local networks in central Italy from 2008 to 2017. The authors used their estimates of both E_R and M_0 to investigate the impact of different magnitude scales on the aleatory variability associated with regional ground-motion prediction equations (Bindi et al., 2019). In this study, we review the procedure for estimating M_0 and E_R from S-wave windows, enlarging the calibration data set. Most importantly, the scientific algorithms are re-engineered to work automatically and to provide outcomes through a web application as presented in the following sections.

RAMONES Web Interface

RAMONES is a service for disseminating seismic moment (M_0) and radiated energy (E_R) computed by applying empirical attenuation models to features extracted from recordings. The service has been active since January 2020 (see Data and Resources), providing the source parameters for earthquakes with local magnitudes M_L larger than about 1.7 recorded within a region bounded by 40.0°N and 44.5°N in latitude and 10.50°E and 16.50°E in longitude. The threshold magnitude was selected following Bindi et al. (2020). These authors analyzed a subset of data considered in this study and found that, given the stations azimuthal and distance distribution in the investigated area, reliable source parameters can be retrieved
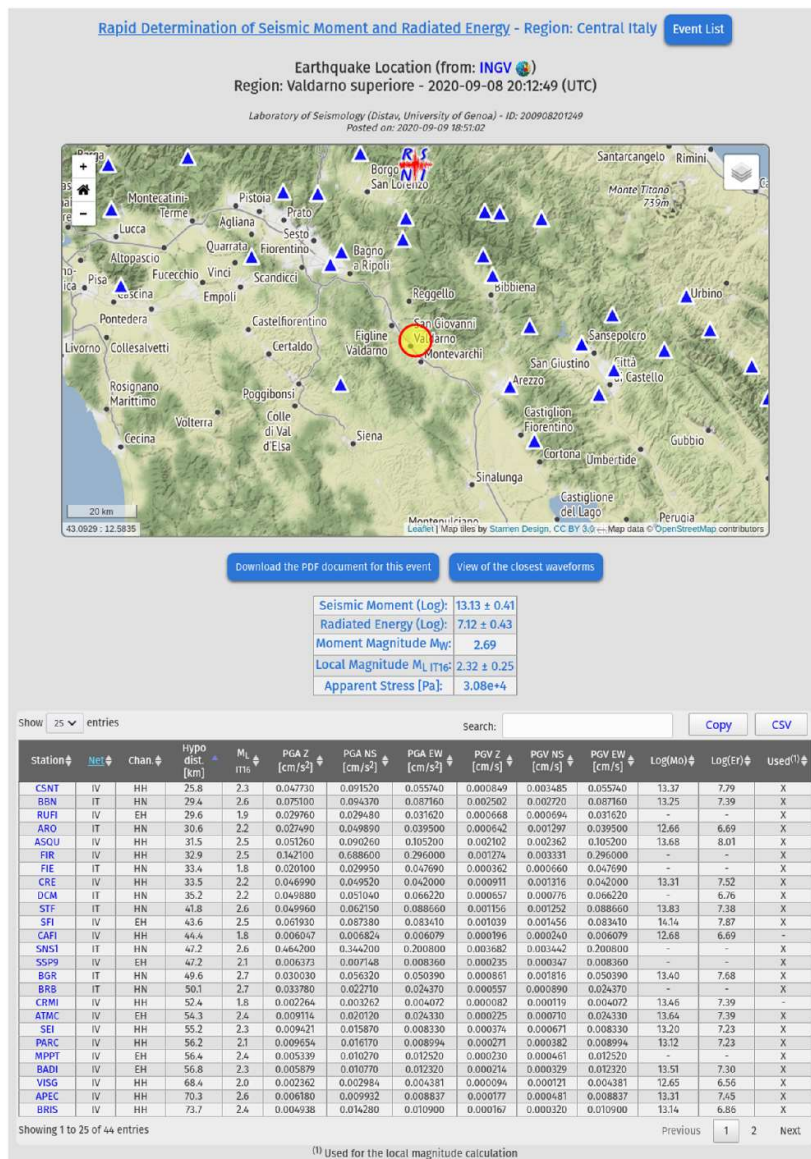
Rapid Determination of Seismic Moment and Radiated Energy - Region: Central Italy [Event List]

Earthquake Location (from: INGV 🌐)
Region: Valdarno superiore - 2020-09-08 20:12:49 (UTC)
Laboratory of Seismology (Distav, University of Genoa) – ID: 200908201249
Posted on: 2020-09-09 18:51:02

[Download the PDF document for this event] [View of the closest waveforms]

Seismic Moment (Log):	13.13 ± 0.41
Radiated Energy (Log):	7.12 ± 0.43
Moment Magnitude M_W:	2.69
Local Magnitude M_L IT16:	2.32 ± 0.25
Apparent Stress [Pa]:	3.08e+4

Show 25 entries   Search: [   ]   [Copy] [CSV]

Station	Net	Chan.	Hypo dist. [km]	M_L IT16	PGA Z [cm/s²]	PGA NS [cm/s²]	PGA EW [cm/s²]	PGV Z [cm/s]	PGV NS [cm/s]	PGV EW [cm/s]	Log(Mo)	Log(Er)	Used[1]
CSNT	IV	HH	25.8	2.3	0.047730	0.091520	0.055740	0.000849	0.003485	0.055740	13.37	7.79	X
BBN	IT	HN	29.4	2.6	0.075100	0.094370	0.087160	0.002502	0.002720	0.087160	13.25	7.39	X
RUFI	IV	EH	29.6	1.9	0.029760	0.029480	0.031620	0.000668	0.000694	0.031620	-	-	X
ARO	IT	HN	30.6	2.2	0.027490	0.049890	0.039500	0.000642	0.001297	0.039500	12.66	6.69	X
ASQU	IV	HH	31.5	2.5	0.051260	0.090260	0.105200	0.002102	0.002362	0.105200	13.68	8.01	X
FIR	IV	HH	32.9	2.5	0.142100	0.688600	0.296000	0.001274	0.003331	0.296000	-	-	X
FIE	IT	HH	33.4	1.8	0.020100	0.029950	0.047690	0.000362	0.000660	0.047690	-	-	X
CRE	IV	HH	33.5	2.2	0.046990	0.049520	0.042000	0.000911	0.001316	0.042000	13.31	7.52	X
DCM	IT	HH	35.2	2.2	0.049880	0.051040	0.066220	0.000657	0.000776	0.066220	-	6.76	X
STF	IT	HN	41.8	2.6	0.049960	0.062150	0.088660	0.001156	0.000240	0.088660	13.83	7.38	X
SFI	IV	EH	43.6	2.5	0.061930	0.087380	0.083410	0.001039	0.001456	0.083410	14.14	7.87	X
CAFI	IV	HH	44.4	1.8	0.006047	0.006824	0.006079	0.000196	0.000240	0.006079	12.68	6.69	-
SNS1	IT	HN	47.2	2.6	0.464200	0.344200	0.200800	0.003682	0.003442	0.200800	-	-	X
SSP9	IV	EH	47.2	2.1	0.006373	0.007148	0.008360	0.000235	0.000177	0.008360	-	-	X
BGR	IT	HN	49.6	2.7	0.030030	0.056320	0.050390	0.000861	0.001816	0.050390	13.40	7.68	X
BRB	IT	HN	50.1	2.7	0.033780	0.022710	0.024370	0.000557	0.000890	0.024370	-	-	X
CRMI	IV	HH	52.4	1.8	0.002264	0.003262	0.004072	0.000082	0.000119	0.004072	13.46	7.39	-
ATMC	IV	EH	54.3	2.4	0.009114	0.020120	0.024330	0.000225	0.000710	0.024330	13.64	7.39	X
SEI	IV	HH	55.2	2.3	0.009421	0.015870	0.008330	0.000374	0.000671	0.008330	13.20	7.23	X
PARC	IV	HH	56.2	2.1	0.009654	0.016170	0.008994	0.000271	0.000382	0.008994	13.12	7.23	X
MPPT	IV	EH	56.4	2.4	0.005339	0.010270	0.012520	0.000230	0.000461	0.012520	-	-	X
BADI	IV	EH	56.8	2.3	0.005879	0.010770	0.012320	0.000214	0.000329	0.012320	13.51	7.30	X
VISG	IV	HH	68.4	2.0	0.002362	0.002984	0.004381	0.000094	0.000121	0.004381	12.65	6.56	X
APEC	IV	HH	70.3	2.6	0.006180	0.009932	0.008837	0.000177	0.000481	0.008837	13.31	7.45	X
BRIS	IV	HH	73.7	2.4	0.004938	0.014280	0.010900	0.000167	0.000320	0.010900	13.14	6.86	X

Showing 1 to 25 of 44 entries   Previous [1] [2] Next

[1] Used for the local magnitude calculation

Figure 2. *Screenshot of the RAMONES event-specific webpage. The epicentral location of the earthquakes (circle) and the station locations (triangles) are shown in a map, and the source parameters and station specific estimates of different ground-motion features (e.g., the peak ground acceleration [PGA] and peak ground velocity [PGV] for the three components) are listed in two different tables. Station specific estimates of seismic moment (M_0) and radiated energy (E_R) are listed as well. See RAMONES Concept section for more details.*

estimate the local magnitude, and to extract different features from the recordings such as the peak displacement and the integral of the squared velocity ($IV2_S$) over the S-wave window, the peak ground velocity (PGV), and peak ground acceleration (PGA). (4) The seismic moment (M_0) and radiated energy (E_R) are estimated using empirical attenuation models derived in this study and are described in the following sections. Furthermore, additional parameters such as apparent stress (σ_a; Wyss and Brune, 1968) and the moment magnitude (M_w, Hanks and Kanamori, 1979) are computed as well. (5) Finally, the results are stored in a PostgresSQL database and disseminated through a web interface. In its current configuration, RAMONES updates are scheduled on a daily basis.

A web portal allows the users to interact with the database. The main page of RAMONES (Fig. 1) includes:

• A map of the monitored region showing the epicenters of earthquakes processed by RAMONES since January 2020. Using the "change selection" option, the geographical extension, the depth and magnitude ranges, and the time span of interest can be configured by the user. In its actual configuration, RAMONES analyzes earthquakes with magnitudes above M_L 1.7 occurring in central Italy.

• Selecting "seismic station," RAMONES shows a table reporting the main information of the stations stored in the database and actually used by the service (more than 570 as of 01 January 2021). In particular, the table includes the following:

○ station information (code, network, channels, latitude, longitude, elevation, and location) including links;

○ link to metadata (dataless);

○ link to an automatically generated summary document (Portable Document file Format [PDF]) showing a map with the station location and horizontal-to-vertical (H/V) spectral ratios for both the S-wave phase window and noise window computed by the service;

○ tools for searching, sorting, and exporting the station table are also available.

• A table reporting the main information of the earthquakes stored in the RAMONES database and the associated source parameters. In particular, the table includes the following:

○ the earthquake location (origin time, latitude, longitude, and depth) provided by the INGV bulletin and a link (ID-INGV) to the INGV event-specific webpage;
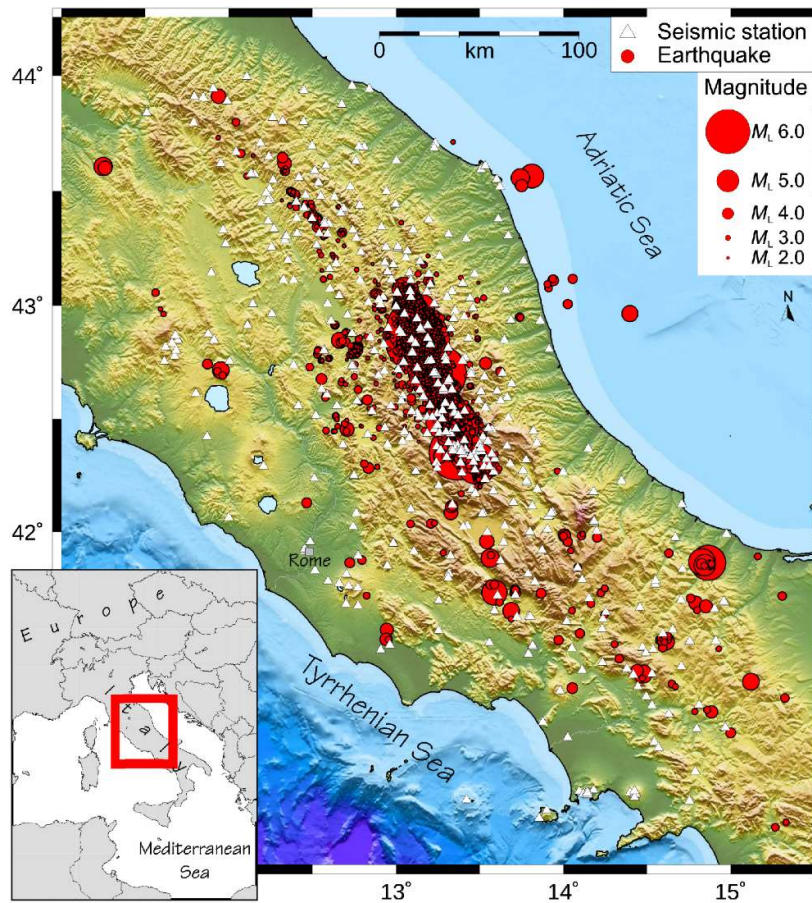
for earthquakes above M_w 1.8–2, without strong bias due to unaccounted attenuation effects.

RAMONES is based on an automatic procedure implemented through the following steps: (1) locations and magnitudes of earthquakes occurring within the target region are retrieved from the National Institute for Geophysics and Volcanology (INGV) bulletin (see Data and Resources), (2) hypocentral information are used to extract segments from continuous data streams archived in the ORFEUS-EIDA, the Incorporated Research Institutions for Seismology (IRIS), and the DPC repositories; only recordings at hypocentral distances shorter than 150 km are downloaded, along with the relevant station metadata. (3) The automatic procedure described in Scafidi et al. (2016) is applied to detect P and S onsets, to

Figure 3. Map showing the earthquake locations (circles) and the station locations (triangles) relevant to the data set used for calibrating and validating the attenuation models implemented by RAMONES. The events on the map cover the time period of 2008–2018 and the local magnitude range of 1.6–6.5. The location of the study area is indicated by the rectangle shown in the inset.

○ Finally, the first three columns provide additional links to the event-specific page (region), to a static image showing a few selected recordings (waves), and to an automatically generated summary document (PDF).

○ Tools for searching, sorting, and exporting the event table are also available.

○ Below the event table, five different figures are automatically updated to summarize the scaling relationships among different source parameters (e.g., scaled energy E_R/M_0 vs. M_w; $\log(E_R)$ vs. $\log(M_0)$; M_{LER} vs. M_{LIT16}). Each panel reports both the values used to calibrate and validate the empirical models (i.e., events occurring before 2020) and those obtained by applying the models to earthquakes occurring after the calibration phase.

Through the link in the first column (region), an event-specific page for the selected event is opened (Fig. 2). This page provides a map with the location of the stations used by RAMONES for processing and the earthquake location; a summary of the source parameters of the selected events; a table listing various information extracted from each recording: the station and network names and the specific channel (using the Standard for the Exchange of Earthquake Data convention for the channel names; see Data and Resources); the hypocentral distance; the station local magnitude; the PGA and PGV over the three components; the station estimates of $\log(M_0)$, and $\log(E_R)$; a flag (used) to indicate whether a record has been used (X) or discarded (-) for the event magnitude calculation (i.e., discarded records have a low signal-to-noise ratio [SNR]). Finally, it is also possible to download the information contained in the event-specific page into a document (PDF) (the same document that can be downloaded from the table in the main page) and to visualize the waveforms of the vertical component recorded at the 10 closest stations.

Calibration Dataset and Processing

The data set used to calibrate the empirical models used by RAMONES consists of 6515 earthquakes located in central Italy (Fig. 3) and recorded by 464 stations. This data set includes broadband, short-period, and accelerometric signals recorded since 2008. The bulk of the data set originates from the 2016 to 2017 central Italy sequence (Chiaraluce et al., 2017) and the 2009 Aquila sequence (Ameri et al., 2009). Data for calibration were collected by the following permanent networks: the National Seismic Network (Rete Sismica Nazionale), operated by
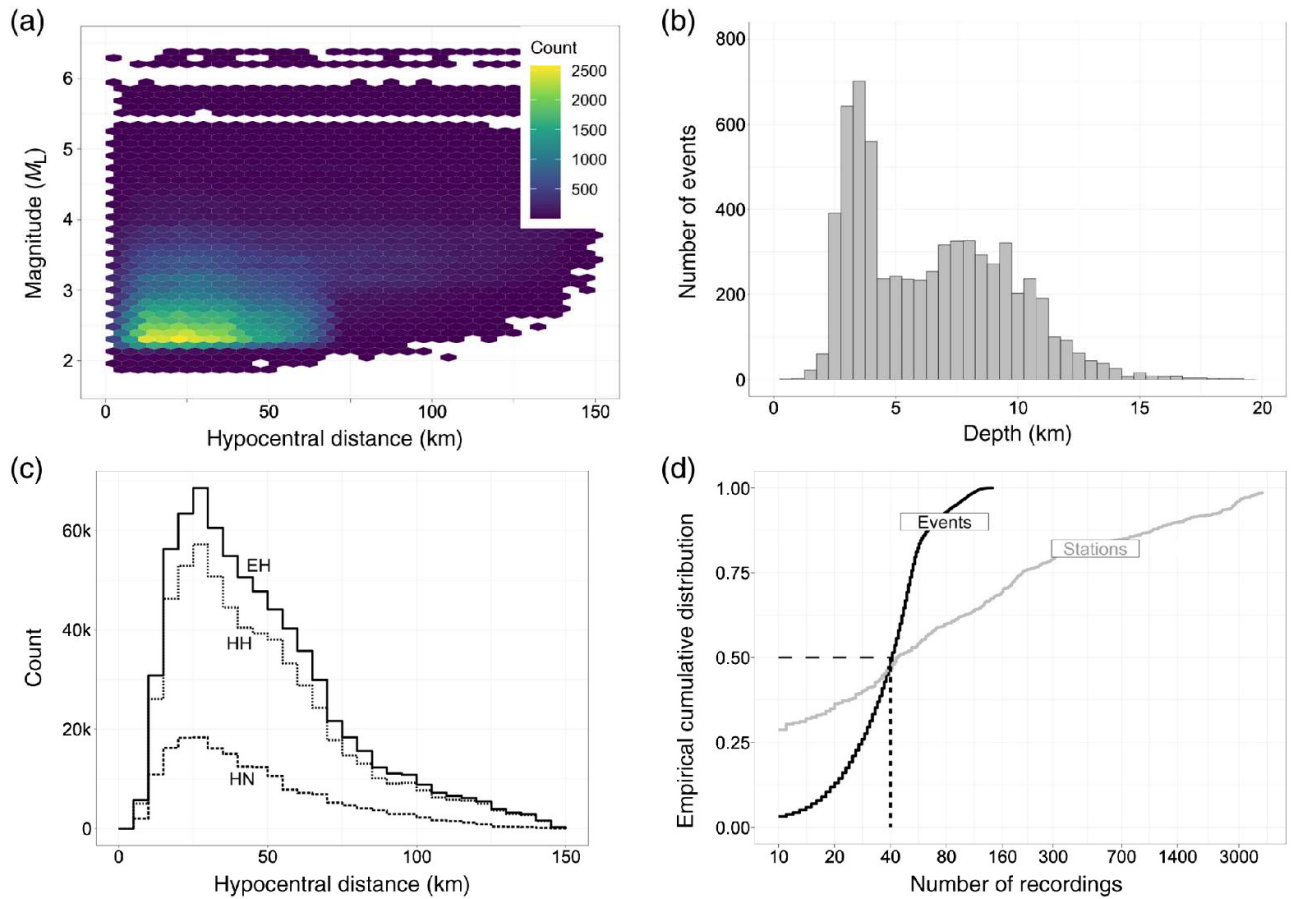
○ the base-10 logarithm of the estimated seismic moment $\log(M_0)$ and radiated energy $\log(E_R)$. The empirical attenuation models used to compute these parameters are described in the following sections;

○ several magnitude estimates are listed. M_L INGV and M_w INGV are the local and moment magnitudes reported by the INGV bulletin; M_{LIT16} is the local magnitude computed considering the attenuation model of Di Bona (2016), but without considering the station corrections: $M_{LIT16} = \log(A) + 1.667 \log(R/100) + 0.001736(R - 100) + 3$, in which A is the geometrical mean of the two horizontal Wood–Anderson amplitudes in millimeters and R is the hypocentral distance; M_w is the moment magnitude computed from our M_0 estimates using Hanks and Kanamori (1979): $M_w = (\log(M_0) - 9.1)/1.5$; M_{LER} is a local magnitude calibrated over $\log(E_R)$, similar to Picozzi et al. (2018), as described in the following sections;

○ The apparent stress σa (Wyss and Brune, 1968) is computed assuming a constant rigidity (μ) in the source area equal to 3×10^4 MPa, considered representative of the average crust conditions for the central Apennines chain.

Figure 4. *Data set used for calibrating the models used by RAMONES for estimating M_0 and E_R. (a) Local magnitude versus hypocentral distance distribution of the considered recordings, (b) distributions of the hypocentral depths, (c) number of recordings used for the HH (broadband), EH (short-period), and HN (accelerometers) channels, and (d) empirical cumulative distribution of the number of recordings per station and per event.*

INGV; Mednet, operated by INGV; and the National Accelerometric Network (Rete Accelerometrica Nazionale), operated by the DPC (see Data and Resources). Stations from temporary networks were also used for calibrating the attenuation models. These include the networks for aftershock monitoring (Margheriti et al., 2011), site effects (Bergamaschi et al., 2011; Cultrera et al., 2016), and seismic microzonation (Gruppo di LavoroMS-AQ, 2010; Cara et al., 2019).

The selected data set is composed of almost 840,000 waveforms (considering the three components of motion) in the M_L range of 1.6–6.5 (Fig. 4a). The hypocentral distances span the range of 5–150 km, with about 50% of the data recorded at hypocentral distances <30 km. Depth shows a bimodal distribution, with peaks at about 3 and 7.5 km (Fig. 4b). Broadband seismometers (i.e., channel HH) and short-period seismometers (channel EH) are often collocated with strong-motion sensors (channel HN), and the distributions with the distance of the number of recordings for the different channels are shown in Figure 4c. In this study, collocated instruments are considered different stations. Details on the instruments and stations of each network are listed in Table S1, available in the supplemental material to this article. About 50% of the stations recorded at least 40 earthquakes and about 50% of the earthquakes have at least 40 records (Fig. 4d). Data selection and processing is made following Pacor et al.

(2016) and Bindi et al. (2018). In particular, an automatic procedure (Spallarossa et al., 2014; Scafidi et al., 2016) is applied for determining the P- and S-wave onsets, and the earthquake location is performed with a nonlinear location algorithm (Lomax et al., 2000), considering a 1D velocity model calibrated for the area with station corrections (Spallarossa et al., 2020).

Aiming to have consistent estimates of the local magnitude for the whole data set, Wood–Anderson seismograms in the hypocentral distance range of 10–150 km are synthesized following Spallarossa et al. (2002). The local magnitude M_{LIT16} is then computed by averaging the station magnitude estimates and considering the zero-magnitude attenuation model calibrated by Di Bona (2016) for Italy, but without applying station corrections. Figure 5 shows the RAMONES processing workflow used to evaluate, for each recording, the S-wave peak displacement (PDS) and the $IV2_S$ over the S-wave window. The workflow follows the procedure developed by Scafidi et al. (2019). The high-pass corner frequency of the predeconvolution filter is automatically determined based on signal-to-noise analysis, selecting the lowest frequency in the 0.3–2.0 Hz range for which the SNR is larger than 4.0. The parameters PDS and $IV2_S$ are computed considering a time window starting 0.1 s before the S-wave onset and ending at different percentages of the cumulated energy as a function of the source to site distance R: (1) 90%
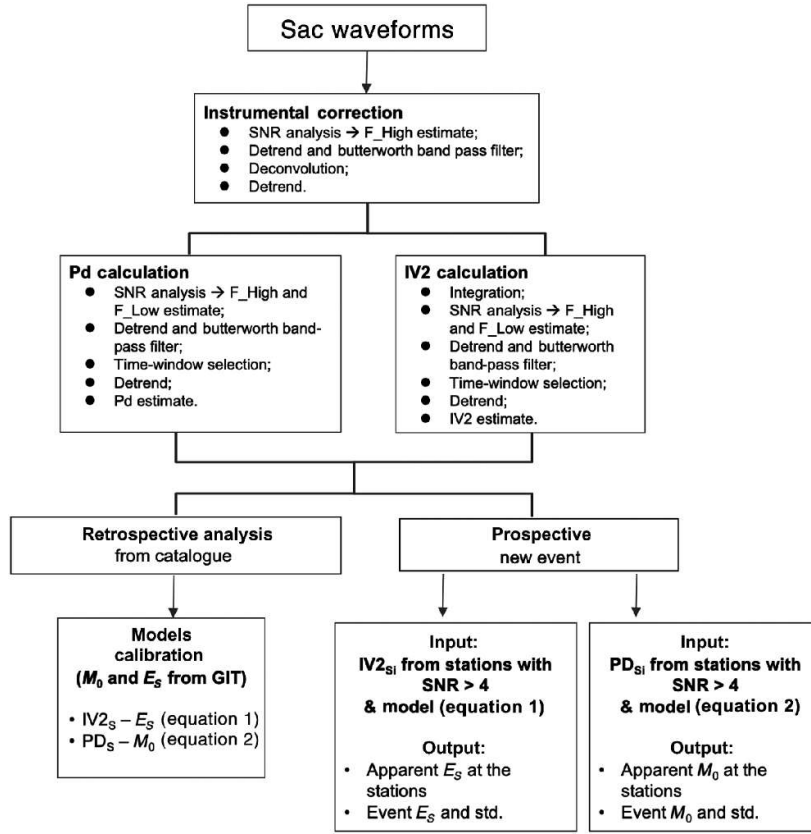
Figure 5. *RAMONES workflow for deriving and applying the empirical models relating the ground-motion features S-wave peak displacement (PDS) and integral of the squared velocity over the S-wave window (IV2$_S$) to the estimates of seismic moment (M_0) and radiated energy (E_R). The RAMONES procedure works on both accelerometric and velocimetric recordings. In the workflow, retrospective analysis indicates the operations performed for calibrating the empirical models starting from the source parameters provided by the spectral decomposition, and prospective analysis indicates the application of the models to new data (operational phase). Notice that F-high (high-pass frequency) and F_low (low-pass frequency) assume different values in the different steps of the process shown in this workflow. GIT, generalized inversion technique; SNR, signal-to-noise ratio.*

and E_R relies on measuring specific ground-motion features directly on seismograms and correcting them for propagation and site effects using empirical models previously calibrated for the region of interest. The source parameters needed to derive the attenuation models are extracted from the FAS of the 6515 earthquakes selected from the central Italy dataset and by applying a spectral decomposition approach known as the generalized inversion technique (GIT) (among others, Andrews, 1986; Castro et al., 1990; Oth et al., 2011). The GIT assumes that the recorded spectra are given by the convolution of source, propagation, and site terms; a factorization of the spectra, expressed as an inverse problem, is possible by exploiting the redundancy of information available when the same event is recorded by different stations located at different distances and the same station is recording several different earthquakes. We apply the GIT in its nonparametric formulation (Castro et al., 1990) and solve the overdetermined linear system of equations in a constrained least-squares sense. Details about the approach applied in central Italy are given by Bindi et al. (2018). Once the nonparametric source spectra are isolated from the other terms, we compute the seismic moment M_0 and the corner frequency (f_c) from the best-fitting omega-square source model (Brune, 1970), assuming an average S-wave radiation pattern $R^{\theta\varphi} = 0.55$ and average density and shear-wave velocity at the source equal to 2700 kg/m³ and 3200 m/s, respectively. Finally, following Izutani and Kanamori (2001) and Venkataraman and Kanamori (2004), we assess the model-dependent radiated energy E_R from the $IV2_S$ Brune source spectra (see also Picozzi et al., 2018; Picozzi, Bindi, Spallarossa, et al., 2019).

Regarding the strong-motion features extracted from seismograms, following Picozzi et al. (2017) and Picozzi, Bindi, Zollo, et al. (2019), we consider the $IV2_S$ time window and PDS. The $IV2_S$ and PDS values relevant to the kth earthquake recorded at the lth station are then linked to E_R and M_0, respectively, through the following empirical attenuation models:

$$\log[IV2_S(R_H)]_{kl} = A + B\log(E_R)_k + w_j C_j + (1-w_j)C_{j+1} + \sum_{i=1}^{N_{sta}} \delta_{il} S_i \quad (1)$$

and

when $R < 25$ km; (2) 80% when 25 km $< R < 50$ km; and (3) 70% when $R > 50$ km. For both PDS and $IV2_S$ calculation, we imposed a minimum time window length of 2.5 s and a maximum time window length of 20 s. For each recording, the SNR was evaluated considering a pre-event noise window of the same length as the direct S waves. The logarithm of both PDS and $IV2_S$ is computed using displacement and velocity band-pass filtered signals; the low-pass and high-pass corner frequencies are computed by SNR analysis, following Scafidi et al. (2016). For calibrating the empirical model describing the scaling of PDS with hypocentral distance and M_0, the estimates of PDS for the north–south and east–west components are averaged (geometric mean). For the scaling of $IV2_S$ with hypocentral distance and E_R, the measures of $IV2_S$ obtained from the three components of ground motion are summed. Figure 6a,b shows the distribution of PDS and $IV2_S$ with respect to hypocentral distance, respectively. Finally, the Fourier amplitude spectra (FAS) are calculated and selected following the procedure described in Pacor et al. (2016).

RAMONES Concept

The concept developed for the rapid assessment of M_0

$$\log[PD_S(R_H)]_{kl} = D + F\log(M_0)_k + w_j G_j$$
$$+ (1 - w_j)G_{j+1} + \sum_{i=1}^{N_{sta}} \delta_{il} Z_i, \qquad (2)$$

in which the hypocentral distance (R_H) range is discretized into N_{bin}; the index $j = 1; \ldots; N_{bin}$ indicates the jth node selected such that R_H is between the distances $r_j \leq R_H < r_j + 1$; the attenuation function is linearized between nodes r_j and $r_j + 1$ using the weights w, computed as $w_j = (r_j + 1 - R_H)/(r_j + 1 - r_j)$ The distance range of 2–150 km is discretized into 50 bins equally spaced on a logarithmic scale. The S_i and Z_i terms are the station correction for station i, and N_{sta} is the number of stations. The coefficients A, B, C_j, D, F, and G_j are determined by solving the overdetermined linear systems (equations 1 and 2) in a least-squares sense. To fix the trade-off between A and C_j, and between C_j and G_j the attenuation is constrained to zero at r_2 equal to 5 km. The station corrections and the coefficients of the attenuation models are reported in Tables S1 and S2, respectively. Positive station corrections are usually related to high-amplification effects as shown in Figure S1 in which two H/V are reported as examples. The calculated regressions have an R2 equal to 0.93 and 0.92, respectively.

The observed $IV2_S$ and PD_S values corrected for the source scaling $A + B\log(E_R)$ and $D + F\log(M_0)$ are compared with the attenuation models C_j and G_j in Figure 7a,b. The high number of events (i.e., ~6500) in the calibration data set, which corresponds to ~210;000 waveforms, made the attenuation models very robust. This is also indicated by the good agreement of the scaling with distance between model parameters and corrected data. Figure 7c,d shows the comparison between the values E_R and M_0 computed by the spectral decomposition with the values obtained correcting $IV2_S$ and PDS for attenuation effects as modeled through the C_j and G_j coefficients. These results suggest that the scaling coefficients A, B and D, F capture well the trend in the data over the entire energy and moment ranges. The station corrections S_j and Z_j are shown in Figure 7e,f, in which the different branches correspond to different station channels.

Following the original idea of Kanamori et al. (1993), the E_R estimates are then used also to derive an energy-based local magnitude scale that agrees with M_{LIT16}. The advantage of calibrating a local magnitude scale on radiated energy (M_{LER}) is that it can be extended toward larger magnitudes without saturation (i.e., differently from the classic M_L scales based on the recording deconvolution for the Wood–Anderson seismograms, M_{LER} is not saturating). The best-fit model that obtained fitting M_{LIT16} as function of $\log(E_R)$ is given by:

$$M_{LER} = 0.56\log(E_R) - 1.80, \qquad (3)$$

with standard deviation of the residuals equal to 0.09 magnitude units. We indicate with M_{LER} the local magnitude obtained by applying equation (3).
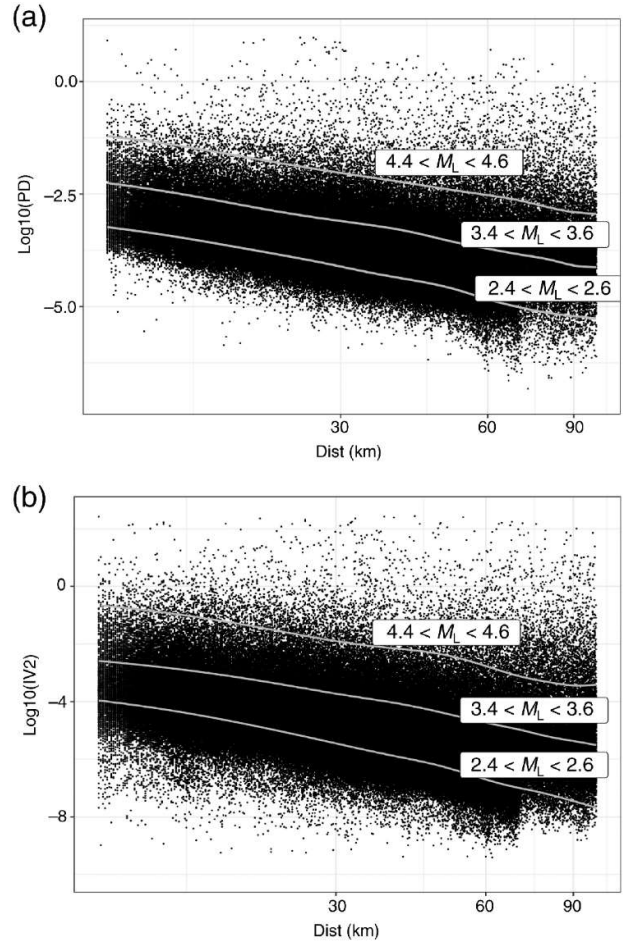

Figure 6. Distribution with hypocentral distance of the (a) peak displacement over the S-wave window and of the (b) IV2S. The trends of the parameters averaged over three narrow magnitude ranges as indicated in the panels (gray line) are also shown.

RAMONES Capabilities

To validate the capabilities of RAMONES, we apply the attenuation models of equations (1) and (2) to a dataset of events that occurred in central Italy during 2019. These earthquakes were considered when performing the GIT inversion but were not considered for the calibration of the attenuation models. This dataset is composed of 60 earthquakes with magnitude M_{LIT16} between 2.3 and 4.7 (Fig. 1a). Figure 8a,b compares the GIT estimates of E_R and M_0 with those retrieved with the RAMONES procedure. A good agreement among spectral estimates and those derived from waveforms analysis is observed over the whole explored range of seismic moment and energy. The $\log(M_0)_{GIT} - \log(M_0)_{RAMONES}$ residual distribution has mean and standard deviation values equal to $1.45 \cdot 10^{-4}$ and 0.2, respectively; the mean and standard deviation for the energy residuals are $6 \cdot 10^{-3}$ and 0.29, respectively. Because equations (1) and (2) are applied to each single recording, it is possible to compare the distribution of the single station RAMONES estimates of E_R and M_0 with the source parameters obtained through the GIT inversion. The residuals between the GIT and RAMONES M_0 and E_R estimates for single recording do not show any particular trend either with hypocentral distance and
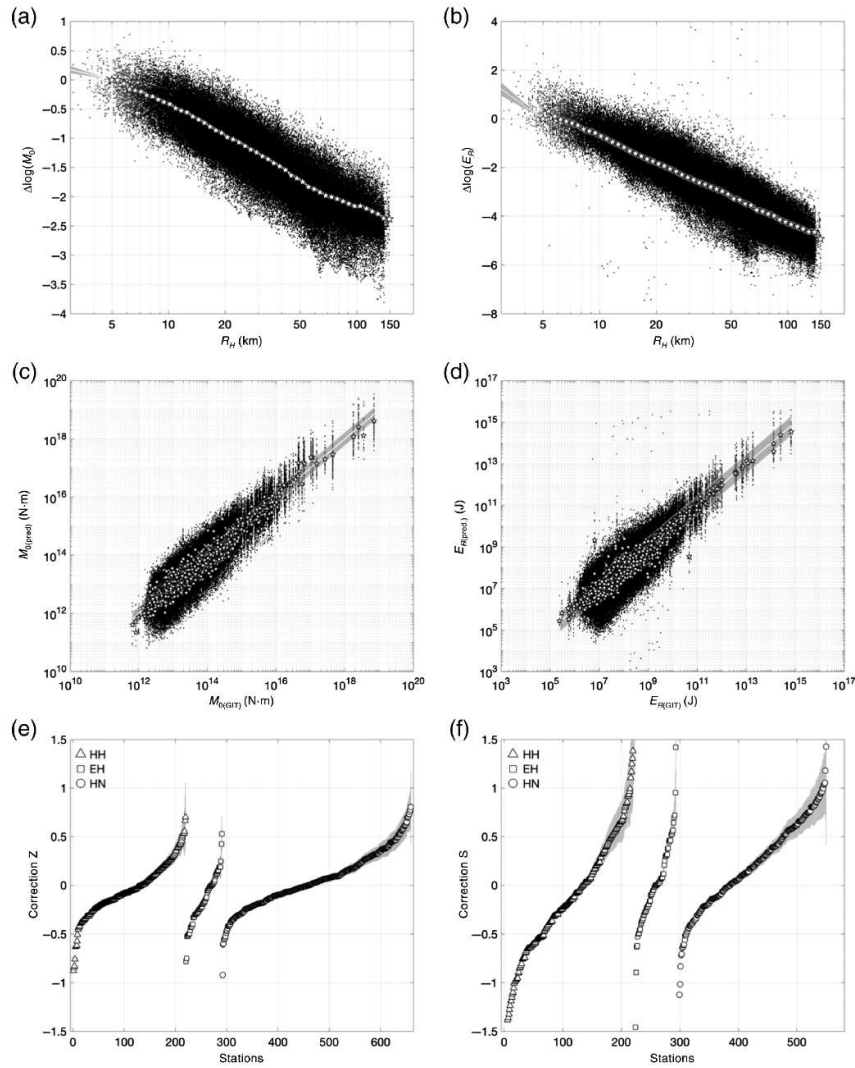
Figure 7. *Results of the calibrations between $IV2_S$ and E_R (equation 1) and between PDS and M_0 (equation 2). (a) The coefficients G_j in equation (2) (white stars) ± 1 standard deviation (gray area) are compared with the residuals $\Delta \log(M_0) = \log[PD_S(R_H)] - D + F \log(M_0)$ (black dots). (b) The same as (a), but for the coefficients C_j of equation (1) (white stars) that are compared with the residuals $\Delta \log(E_R) = \log[IV2_S(R_H)] - A + B \log(E_R)$ (black dots). (c) PD_S values corrected for G_j are compared with $M_0(obs)$ (the corrected values for each recording are in black, and the average for each earthquake is plotted as a white star). (d) The same as (c), but $IV2_S$ values corrected for C_j are compared with the energy $E_R(obs)$. (e) Station correction coefficients Z_i (equation 2). (f) The same as (e), but for station correction coefficients S_i (equation 1). Station corrections are reported in Table S1.*

depth (Fig. 8c–f) or with magnitude (Fig. 8g,h). We observe a larger dispersion for seismic energy estimates (residuals standard deviation for E_R and M_0 is 0.29 and 0.2, respectively), in agreement with the larger variability observed for the energy during the model calibration.

Between January and September 2020, RAMONES computed the source parameters of about 800 earthquakes that occurred in central and southern Apennines, Italy (Fig. S2). Figure 9 shows the scaling of the seismic energy E_R with moment M_0. Gray squares indicate data produced by the RAMONES service in the period January–September 2020, and black dots indicate the calibration data set (2008–2018). During the testing phase in 2020, the RAMONES procedure is applied also to stations not considered during the calibration phase. Site specific adjustments in equations (1) and (2) for these stations are set to zero, and they can be determined once enough local earthquakes have been recorded in the magnitude and distance ranges of interest. Similar to the procedure suggested to determine the local magnitude adjustments of new broadband or strong-motion stations installed in California (Uhrhammer et al., 2011), the statistical analysis of the residual distribution can provide robust estimates of the median corrections and their uncertainties.

Future Perspectives
For testing its performances and for evaluating its potentiality, RAMONES has been running since January 2020 with a configuration set to daily updates (Fig. S2). For its long-term operability, several changes and developments in the operational configuration are possible. For rapid response actions, RAMONES provides information about the seismic radiation of sources, which is better related to the shaking potential of the earthquake than the size given by the seismic moment (Di Giacomo and Bormann, 2011). Future studies will explore the information
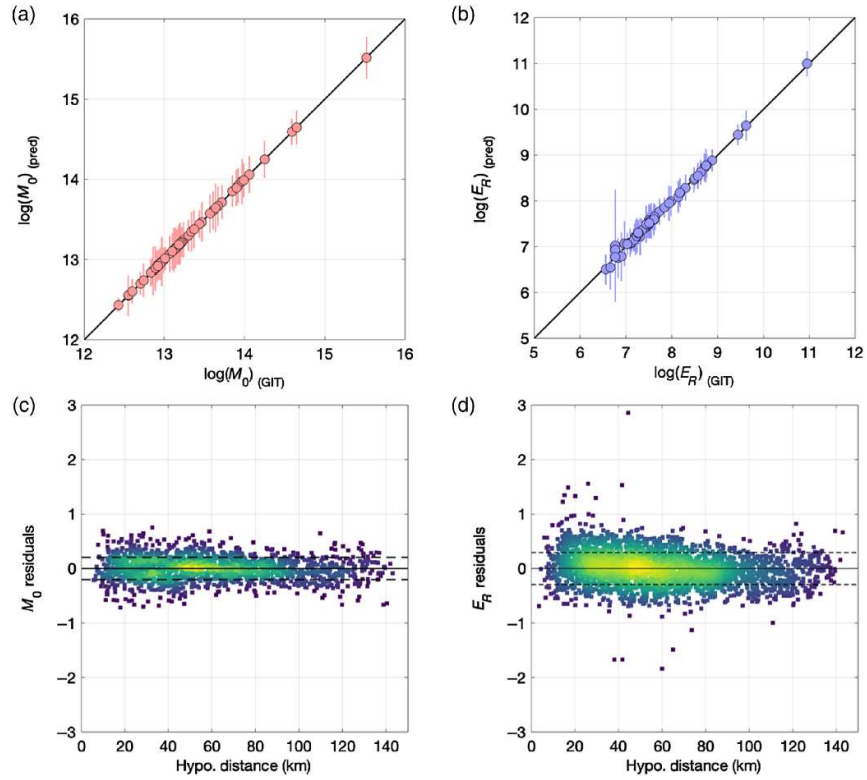
Figure 8. *Comparison of E_R and M_0 estimates obtained from the GIT and RAMONES for 2019 earthquakes data. (a) $\log(M_0)$ from the GIT versus RAMONES; ±1 standard deviation for RAMONES estimates (colored vertical bars) and 1:1 scaling relation (black line). (b) The same as (a), but for $\log(E_R)$. (c) Residuals between the GIT and RAMONES for $\log(M_0)$ estimates for single recording with hypocentral distance (dots colored per density of data); ±1 standard deviation (black dashed lines). (d) The same as (c), but for $\log(E_R)$ residuals. (e) and (f) the same as (d) and (c), respectively, but for magnitude. (g) and (h) the same as (d) and (c), respectively, but for hypocentral depth. (Continued)*

Figure 8. *Continued.*

9

Last update: 2020-09-27 11:41:49
Last event: Scapoli (IS), 2020-09-26 22:32:07, M_L:2.3 [INGV]
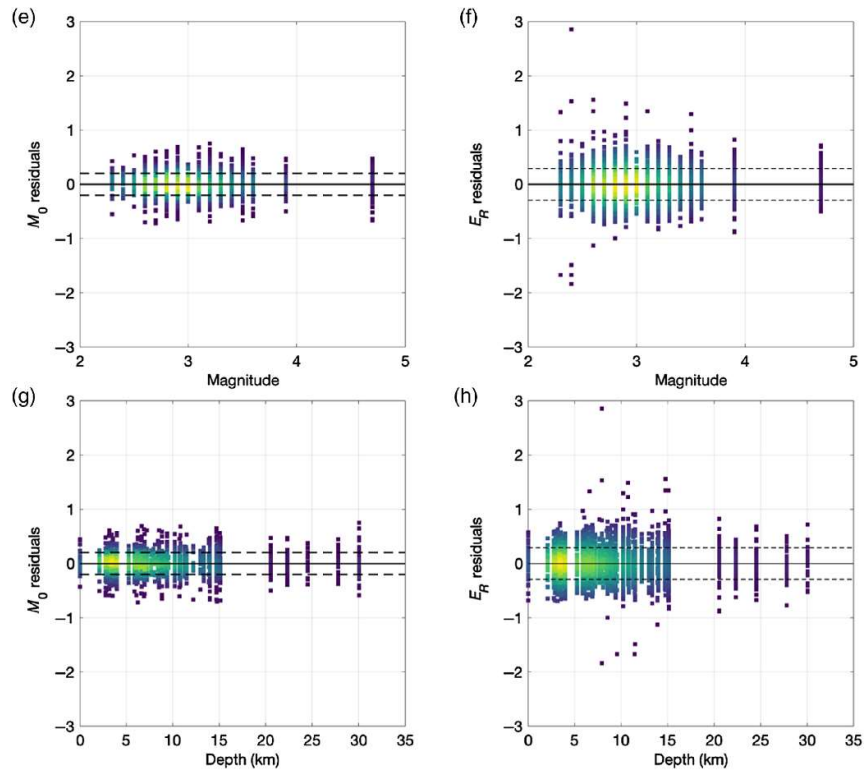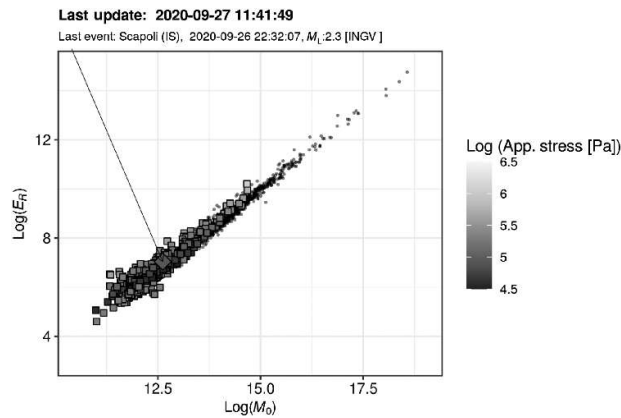
Figure 9. *Scaling of the seismic energy E_R with moment M_0. Gray squares indicate the RAMONES data set (from January to September 2020), and black dots are relevant to the calibration data set (2008–2018).*

provided by RAMONES (e.g., apparent stress) to improve the consistency between the observed and predicted shaking levels used for generating shaking maps. The high potential of RAMONES is in its ability to provide timely information on the temporal evolution of static and dynamic source parameters. This could be particularly useful during a seismic sequence, for a change in the source dynamics provides information on the mechanics of earthquake ruptures. Therefore, for rapid response applications, the RAMONES computations can be switched to a modality triggered by alerting messages such as those issued by the EMSC. Other lines of development for RAMONES regard data accessibility and the extension of the monitored region. Regarding the modalities to retrieve data from RAMONES, future effort will be dedicated to making operative representational state transfer (RESTful) webservices, preserving as much as possible the compatibility with FDSN standards for event, station, and data-select queries, and developing ad hoc dictionaries when needed. As a positive impact, the accessibility through webservices will make possible the interoperability of RAMONES with several other seismological services operating in Europe. To extend the applicability of RAMONES to other regions, new attenuation models for estimating E_R and M_0 from PD_S and $IV2_S$ have to be developed, following the example of the harmonized local magnitude for Europe (Bindi et al., 2019). In conclusion, RAMONES represents, in our opinion, a fine example of how the open-data policy pursued by the European seismological community since the last decade stimulated the growth of applications and services, which in the long term can have a significant impact on mitigating seismic risk.

Data and Resources
We used data and information retrieved from the Observatories and Research Facilities for European Seismology European Integrated Data Archive (https://www.orfeus-eu.org/data/eida/), the Incorporated Research Institutions for Seismology (IRIS) (https://www.iris.edu/hq/), and the Italian Civil Protection Department (http://ran.protezionecivile.it/EN/index.php). The National Institute for Geophysics and Volcanology (INGV) bulletin is used to guide the data download (webservices.rm.ingv.it/fdsnws/event/1/) and to extract the earthquake locations. The International Federation of Digital Seismograph Networks specifications are available at http://www.fdsn.org/ and the Standard for the Exchange of Earthquake Data manual is available at http://www.fdsn.org/pdf/SEEDManual_V2.4.pdf. For the calibration of the attenuation models, we used data mainly from networks IV (INGV Seismological Data Centre, 2006), IT (Presidency of Council Of Ministers-Civil Protection Department, 1972), and MN (MedNet Project Partner Institutions, 1990). In the application phase, although 85% of data were provided by IV and 11% by IT, we also processed data provided by the GU (University of Genova, 1967), OT (University Of Bari "Aldo Moro", 2013), GE (GEOFON Data Centre, 1993), VD (CNR IMAA Consiglio Nazionale Delle Ricerche, Italy, 2019), and IX networks. The map in Figure 1 was prepared with the Generic Mapping Tools software package (http://gmt.soest.hawaii.edu/); R (R Core Team, 2018) and MATLAB R2019b (https://www.mathworks.com/products/matlab.html) were used for the regression analysis and for preparing the figures. The Rapid Assessment of MOmeNt and Energy Service (RAMONES) service is available at http://www.distav.unige.it/rsni/ramones.php. All websites were last accessed in January 2021. The supplemental material contains information about instruments and stations (Table S1), coefficients of the attenuation models (Table S2), and horizontal-to-vertical spectral ratio (H/V) for two stations (Fig. S1), as well as a map (Fig. S2) showing the location of the events automatically elaborated by RAMONES between January and September 2020.

Declaration of Competing Interests
The authors acknowledge that there are no conflicts of interest recorded.

References
Ameri, G., M. Massa, D. Bindi, E. D'Alema, A. Gorini, L. Luzi, M. Marzorati, F. Pacor, R. Paolucci, R. Puglia, et al. (2009). The 6 April 2009 Mw 6.3 L'Aquila (central Italy) earthquake: Strong-motion observations, Seismol. Res. Lett. 80, 951–966.

Andrews, D. J. (1986). Objective determination of source parameters and similarity of earthquakes of different size, in Earthquake Source Mechanics, S. Das, J. Boatwright, and C. H. Scholz (Editors), American Geophysical Union, Washington, D.C., 259–267.

Bergamaschi, F., G. Cultrera, L. Luzi, R. M. Azzara, G. Ameri, P.

Augliera, P. Bordoni, F. Cara, R. Cogliano, E. D'Alema, et al. (2011). Evaluation of site effects in the Aterno river valley (Central Italy) from aftershocks of the 2009 L'Aquila earthquake, Bull. Earthq. Eng. 9, 697–715.

Bindi, D., D. Spallarossa, M. Picozzi, and P. Morasca (2020). Reliability of source parameters for small events in Central Italy: Insights from spectral decomposition analysis applied to both synthetic and real data, Bull. Seismol. Soc. Am. 110, 1–19, doi: 10.1785/0120200126.

Bindi, D., D. Spallarossa, M. Picozzi, D. Scafidi, and F. Cotton (2018). Impact of magnitude selection on Aleatory variability associated with ground-motion prediction equations: Part I-Local, energy, and moment magnitude calibration and stress-drop variability in Central Italy, Bull. Seismol. Soc. Am. 108, no. 3A, 1427–1442, doi: 10.1785/0120170356.

Bindi, D., R. Zaccarelli, A. Strollo, and D. Di Giacomo (2019). Harmonized local magnitude attenuation function for Europe using the European integrated data archive (EIDA), Geophys. J. Int. 218, no. 1, 519–533.

Brune, J. N. (1970). Tectonic stress and the spectra of shear waves from earthquakes, J. Geophys. Res. 75, 4997–5009.

Cara, F., G. Cultrera, G. Riccio, S. Amoroso, P. Bordoni, A. Bucci, E. D'Alema, M. D'Amico, L. Cantore, S. Carannante, et al. (2019). Temporary dense seismic network during the 2016 Central Italy seismic emergency for microzonation studies, Sci. Data 6, 182, doi: 10.1038/s41597-019-0188-1.

Castro, R. R., J. G. Anderson, and S. K. Singh (1990). Site response, attenuation and source spectra of S waves along the Guerrero, Mexico, subduction zone, Bull. Seismol. Soc. Am. 80, 1481–1503.

Chiaraluce, L., R. Di Stefano, E. Tinti, L. Scognamiglio, M. Michele, E. Casarotti, M. Cattaneo, P. De Gori, C. Chiarabba, G. Monachesi, et al. (2017). The 2016 Central Italy seismic sequence: A first look at the mainshocks, aftershocks, and source models, Seismol. Res. Lett. 88, 757–771, doi: 10.1785/0220160221.

CNR IMAA Consiglio Nazionale Delle Ricerche (Italy) (2019). High agri valley geophysical observatory [Data set], International Federation of Digital Seismograph Networks, doi: 10.7914/SN/VD.

Cultrera, G., E. D'Alema, S. Amoroso, B. Angioni, P. Bordoni, L. Cantore, F. Cara, A. Caserta, R. Cogliano, M. D'Amico, et al. (2016). Site effect studies following the 2016 Mw 6.0 Amatrice earthquake (Italy): The Emersito task force activities, Ann. Geophys. 59, doi: 10.4401/ag-7189.

Di Bona, M. (2016). A local magnitude scale for crustal earthquakes in Italy, Bull. Seismol. Soc. Am. 106, 242–258.

Di Giacomo, D., and P. Bormann (2011). The moment magnitude M_w and the energy magnitude Me: Common roots and differences, J. Seismol. 15, 411–427.

GEOFON Data Centre (1993). GEOFON seismic network, Deutsches GeoForschungsZentrum GFZ, Potsdam, Germany, doi: 10.14470/TR560404.

Gruppo di Lavoro MS-AQ (2010). Microzonazione sismica per la ricostruzione dell'area aquilana, Working group coordinated by the Italian Civil Protection, Abruzzo region, 2 vols., and 1 DVD (in Italian).

Hanks, T. C., and H. Kanamori (1979). A moment magnitude scale, J. Geophys. Res. 84, 2348–2350, doi: 10.1029/JB084iB05p02348.

INGV Seismological Data Centre (2006). Rete sismica nazionale (RSN), Istituto Nazionale di Geofisica e Vulcanologia (INGV), Rome, Italy, doi: 10.13127/SD/X0FXnH7QfY.

Izutani, Y., and H. Kanamori (2001). Scale-dependence of seismic energy-to-moment ratio for strike-slip earthquakes in Japan, Geophys. Res. Lett. 28, 4007–4010.

Kanamori, H. (2005). Real-time seismology and earthquake damage mitigation, Annu. Rev. Earth Planet. Sci. 33, 195–214, doi: 10.1146/annurev.earth.33.092203.122626.

Kanamori, H., E. Hauksson, L. K. Hutton, and L. M. Jones (1993). Determination of earthquake energy release and M L using TERRAscope, Bull. Seismol. Soc. Am. 83, 330–346.

Kong, Q., D. T. Trugman, Z. E. Ross, M. J. Bianco, B. J. Meade, and P. Gerstoft (2019). Machine learning in seismology: Turning data into insights, Seismol. Res. Lett. 90, no. 1, 3–14, doi: 10.1175/0220180259.

Lomax, A., J. Virieux, P. Volant, and C. Thierry-Berge (2000). Probabilistic earthquake location in 3D and layered models, in Advances in Seismic Event Location, C. H. Thurber and N. Rabinowitz (Editors), Kluwer Academic Publishers, Dordrecht, The Netherlands/Boston, Massachusetts/London, United Kingdom, 101–134.

Margheriti, L., L. Chiaraluce, C. Voisin, G. Cultrera, A. Govoni, M. Moretti, P. Bordoni, L. Luzi, R. Azzara, L. Valoroso, et al. (2011). Rapid response seismic networks in Europe: Lessons learnt from the L'Aquila earthquake emergency, Ann. Geophys. 54, no. 4, 392–399.

MedNet Project Partner Institutions (1990). Mediterranean very broadband seismographic network (MedNet), Istituto Nazionale di Geofisica e Vulcanologia (INGV), Rome, Italy, doi: 10.13127/SD/fBBBtDtd6q.

Mousavi, S. M., W. Zhu, W. Ellsworth, and G. Beroza (2019). Unsupervised clustering of seismic signals using deep convolutional autoencoders, Geosci. Rem. Sens. Lett. IEEE 16, no. 11, 1693–1697, doi: 10.1109/LGRS.2019.2909218.

Mousavi, S. M., W. Zhu, Y. Sheng, and G. C. Beroza (2019). CRED: A deep residual network of convolutional and recurrent units for earthquake signal detection, Sci. Rep. 9, no. 1, 10,267.

Münchmeyer, J., D. Bindi, C. Sippl, U. Leser, and F. Tilmann (2019). Low uncertainty multifeature magnitude estimation with 3-D corrections and boosting tree regression: Application to North Chile, Geophys. J. Int. 220, no. 1, 142–159.

Nolet, G., B. Romanovicz, R. Kind, and E. Wielandt (1986). The ORFEUS Science Plan, D. Reidel Publishing Co., Dordrecht, The Netherlands, 45 pp.

Oth, A., D. Bindi, S. Parolai, and D. Di Giacomo (2011). Spectral analysis of K-NET and KiK-net data in Japan. Part II: On attenuation characteristics, source spectra, and site response of borehole and surface stations, Bull. Seismol. Soc. Am. 101, 667–687.

Pacor, F., D. Spallarossa, A. Oth, L. Luzi, R. Puglia, L. Cantore, A. Mercuri, M. D'Amico, and D. Bindi (2016). Spectral models for ground motion prediction in the L'Aquila region (central Italy): Evidence for stress-drop dependence on magnitude and depth, Geophys. J. Int. 204, 697–718.

Picozzi, M., D. Bindi, P. Brondi, D. Di Giacomo, S. Parolai, and A. Zollo (2017). Rapid determination of P wave- based energy magnitude: Insights on source parameter scaling of the 2016 Central Italy earthquake sequence, Geophys. Res. Lett. 44, 4036–4045.

Picozzi, M., D. Bindi, D. Spallarossa, D. Di Giacomo, and A. Zollo (2018). A rapid response magnitude scale for timely assessment of the high frequency seismic radiation, Sci. Rep. 8, 8562, doi: 10.1038/s41598-018-26938-9.

Picozzi, M., D. Bindi, D. Spallarossa, A. Oth, A. Di Giacomo, and A. Zollo (2019). Moment and energy magnitudes: Diversity of views on earthquake shaking potential and earthquake statistics, Geophys. J. Int. 216, 1245–1259, doi: 10.1093/gji/ggy488.

Picozzi, M., D. Bindi, A. Zollo, G. Festa, and D. Spallarossa (2019). Detecting long-lasting transients of earthquake activity on a fault system by monitoring apparent stress, ground motion and clustering, Sci. Rep. 9, 16,268, doi: 10.1038/s41598-019-52756-8.

Presidency of Council of Ministers-Civil Protection Department (1972). Italian strong motion network, Presidency of Council of Ministers – Civil Protection Department, doi:

10.7914/SN/IT.

R Core Team (2018). R: A language and environment for statistical computing, R Foundation for statistical computing, Vienna, Austria, available at https://www.r-project.org/ (last accessed June 2018).

Ross, Z. E., E. Hauksson, and Y. Ben-Zion (2017). Abundant off-fault seismicity and orthogonal structures in the San Jacinto fault zone, Sci. Adv. 3, no. 3, e1601946, doi: 10.1126/sci-adv.1601946.

Ross, Z. E., D. T. Trugman, E. Hauksson, and P. M. Shearer (2019). Searching for hidden earthquakes in Southern California, Science 364, no. 6442, 767–771, doi: 10.1126/science.aaw6888.

Scafidi, D., D. Spallarossa, G. Ferretti, S. Barani, B. Castello, and L. Margheriti (2019). A complete automatic procedure to compile reliable seismic catalogs and travel-time and strong-motion parameters datasets, Seismol. Res. Lett. 90, no. 3, 1308–1317, doi: 10.1785/0220180257.

Scafidi, D., D. Spallarossa, C. Turino, G. Ferretti, and A. Viganò (2016). Automatic P- and S-wave local earthquake tomography: Testing performance of the automatic phase-picker engine RSNI-Picker, Bull. Seismol. Soc. Am. 106, no. 2, 526–536, doi: 10.1785/0120150084.

Spallarossa, D., D. Bindi, P. Augliera, and M. Cattaneo (2002). An ML scale in northwestern Italy, Bull. Seismol. Soc. Am. 92, 2205–2216.

Spallarossa, D., M. Cattaneo, D. Scafidi, M. Michele, L. Chiaraluce, M. Segou, and I. Main (2020). An automatically generated high-resolution seismic catalogue for the 2016-2017 Central Italy sequence, including P and S phase arrival times, Geophys. J. Int. doi: 10.1093/gji/ggaa604.

Spallarossa, D., G. Ferretti, D. Scafidi, C. Turino, and M. Pasta (2014). Performance of the RSNI-Picker, Seismol. Res. Lett. 85, 1243–1254, doi: 10.1785/0220130136.

Uhrhammer, R. A., M. Hellweg, K. Hutton, P. Lombard, A. W. Walters, E. Hauksson, and D. Oppenheimer (2011). California integrated seismic network (CISN) local magnitude determination in California and vicinity, Bull. Seismol. Soc. Am. 101, 2685–2693.

University of Bari "Aldo Moro" (2013). OTRIONS, Seismic networks of Gargano Area (Italy), International Federation of Digital Seismograph Networks, doi: 10.7914/SN/OT.

University of Genova (1967). Regional seismic network of North Western Italy, International Federation of Digital Seismograph Networks, doi: 10.7914/SN/GU.

Venkataraman, A., and H. Kanamori (2004). Observational constraints on the fracture energy of subduction zone earthquakes, J. Geophys. Res. 109, no. B05302, doi: 10.1029/2003JB002549.

Wyss, M., and J. N. Brune (1968). Seismic moment, stress, and source dimensions for earthquakes in the California–Nevada region, J. Geophys. Res. 73, 4681–4694.

Zhang, M., W. L. Ellsworth, and G. C. Beroza (2019). Rapid earthquake association and location, Seismol. Res. Lett. 90, no. 6, 2276–2284, doi: 10.1785/0220190052.

Zhu, W., and G. C. Beroza (2018). PhaseNet: A deep-neural-network-based seismic arrival time picking method, Geophys. J. Int. 216, no. 1, 261–273.